

Proton Pandemonium: A first look at the $^{31}\text{Cl}(\beta p \gamma)^{30}\text{P}$ decay scheme

T. Budner,^{1,2,*} M. Friedman,^{3,4} L. J. Sun,^{2,5} C. Wrede,^{1,2,†} B. A. Brown,^{1,2} D. Pérez-Loureiro,³ J. Surbrook,^{1,2} A. Adams,^{1,2} Y. Ayyad,^{3,6} D. W. Bardayan,⁷ K. Chae,⁸ A. A. Chen,⁹ K. A. Chipps,^{10,11} M. Cortesi,² B. Glassman,^{1,3} M. R. Hall,⁷ M. Janasik,^{1,3} J. Liang,⁹ P. O'Malley,⁷ E. Pollacco,¹² A. Psaltis,¹³ J. Stomps,^{1,3} and T. Wheeler^{1,2}

¹*Department of Physics and Astronomy, Michigan State University, East Lansing, MI 48824, USA*

²*Facility for Rare Isotope Beams, Michigan State University, East Lansing, MI 48824, USA*

³*National Superconducting Cyclotron Laboratory, Michigan State University, East Lansing, MI 48824, USA*

⁴*Racah Institute of Physics, Hebrew University, Jerusalem, Israel 91904*

⁵*School of Physics and Astronomy, Shanghai Jiao Tong University, Shanghai 200240, China*

⁶*IGFAE, Universidade de Santiago de Compostela, E-15782 Santiago de Compostela, Spain*

⁷*Department of Physics and Astronomy, University of Notre Dame, Notre Dame, IN 46556, USA*

⁸*Department of Physics, Sungkyunkwan University, Suwon 440-746, Republic of Korea*

⁹*Department of Physics and Astronomy, McMaster University, Hamilton, ON L8S 4L8, Canada*

¹⁰*Physics Division, Oak Ridge National Laboratory, Oak Ridge, TN 37830-37831, USA*

¹¹*Department of Physics and Astronomy, University of Tennessee, Knoxville, TN 37996, USA*

¹²*Département de Physique Nucléaire, IRFU, CEA,*

Université Paris-Saclay, F-91191, Gif-sur-Yvette, France

¹³*Department of Physics and Astronomy, Saint Mary's University, Halifax, NS B3H 3C3, Canada*

(Dated: October 7, 2025)

Background: Positron decays of proton-rich nuclides exhibit large Q values, producing complex cascades which often involve various radiations, including protons and γ rays. Often, only one of the two are measured in a single experiment, limiting the accuracy and completeness of the decay scheme. An example is ^{31}Cl , for which protons and γ rays have been measured in detail individually but never with substantial sensitivity to proton- γ coincidences.

Purpose: Provide detailed measurements of ^{31}Cl β -delayed proton decay including $\beta - p - \gamma$ sequences, extract spectroscopic information on ^{31}S excited states as well as their β feeding, and compare to shell-model calculations.

Methods: A fast, fragmented beam of ^{31}Cl provided by the National Superconducting Cyclotron Laboratory (NSCL) was deposited in the Gaseous Detector with Germanium Tagging (GADGET) system. GADGET's gas-filled Proton Detector was used to detect β -delayed protons, and the Segmented Germanium Array (SeGA) was used to detect β -delayed γ rays.

Results: Up to 18 previously unobserved β -delayed proton transitions have been discovered, most of which populate excited states of ^{30}P . The first detailed $^{31}\text{Cl}(\beta p \gamma)^{30}\text{P}$ decay scheme is presented, including updated β -delayed, proton-decay energies and intensities. Improved agreement is found with theoretical calculations of the summed Gamow-Teller (GT) strength distribution for ^{31}S excitation energies $7.5 < E_x < 9.5$ MeV.

Conclusions: The present work demonstrates that the capability to detect β -delayed protons and γ rays in coincidence is essential to construct accurate positron decay schemes for comparison to theoretical nuclear structure calculations. In some respects, this phenomenon for β -delayed protons resembles the pandemonium effect originally introduced for β -delayed γ rays.

I. INTRODUCTION

Experimental measurements employing β -decay spectroscopy serve as sensitive probes for studying the structure of atomic nuclei located far from the valley of stability. Specifically, extracting the GT strength distribution from experimental data allows for a detailed comparison with shell-model theory. However, as the Q value increases, so does the number of possible transitions, fragmenting the β -decay intensity across many highly-excited, closely-spaced levels in the daughter nucleus. This reduces the experimental sensitivity to detect distinct photopeaks corresponding to primary γ -ray transitions from particular excited states, since the decay intensity is smeared across a broader range of energies. The problem is further exacerbated by the fact that γ -ray detection efficiency tends to decrease with increasing

γ energy. In the present work, we investigate an experimental case similar to this well-known “pandemonium effect” in the context of β -delayed proton emission [1].

The β -delayed γ and proton decay of neutron-deficient ^{31}Cl has been used to measure crucial resonances for constraining the thermonuclear rate of the $^{30}\text{P}(p, \gamma)^{31}\text{S}$ reaction at peak classical nova temperatures [2–7]. The present work is based on the dataset obtained at NSCL using the GADGET system during the ^{31}Cl β^+ decay measurement described in Ref. [7]. This previous study focused on the astrophysical implications of one particular low-energy, $\ell = 0$ resonance. At present, we provide exhaustive analysis of the information-rich coincidence spectra from higher-energy protons and $^{30}\text{P}^*$ γ rays collected during NSCL Experiment 17024. Analysis of high-statistics, proton- γ coincidence data has enabled the discovery of many previously unobserved transitions, as well

as the identification of several new proton-unbound ^{31}S levels. We present the most detailed study of ^{31}Cl β -delayed proton decay to date, reveal the first construction of a $^{31}\text{Cl}(\beta p\gamma)^{30}\text{P}$ decay scheme, and compare these experimental results to theoretical calculations of the GT strength distribution.

II. PREVIOUS SPECTROSCOPIC STUDIES

The 2.5-min half-life of ^{30}P excludes its use as a target for direct-reaction experiments [8], and the lack of high-intensity ^{30}P beams at the astrophysically relevant low energies prohibits measuring the $^{30}\text{P}(p, \gamma)^{31}\text{S}$ reaction in inverse kinematics. However, various indirect methods have been used to study the proton-unbound states of ^{31}S , including single-nucleon transfer [9–13] and charge-exchange reaction measurements [11, 14–16], as well as in-beam γ -ray [17–20] and β^+ spectroscopy [2–5]. The context surrounding the status of $^{31}\text{S}^*$ studies as of 2016 is summarized in Ref. [4] and was extended upon by Bennett *et al.* The original work contained within Ref. [6] details the highest-statistics $^{31}\text{Cl}(\beta\gamma)^{31}\text{S}$ measurement to date. Since then, further experimental results have been published on the reactions $^{32}\text{S}(p, d)^{31}\text{S}$ [21, 22] and $^3\text{He}(^{32}\text{S}, \alpha)^{31}\text{S}$ [23], as well as the radioactive decay $^{31}\text{Cl}(\beta p)^{30}\text{P}$ [7].

Proton emission from ^{31}S levels populated by ^{31}Cl β^+ decay was first observed by Åysto *et al.*, reporting up to eight different proton decay branches in Refs. [24–26]. Subsequent studies confirmed the observation of two ^{31}Cl β -delayed proton decays, attributing the other transitions to contaminant decays [27]. The first application of ^{31}Cl β^+ decay as a probe of potentially crucial resonances for $^{30}\text{P}(p, \gamma)^{31}\text{S}$ was performed by Kankainen *et al.* [2], identifying a total of about a dozen β -delayed proton decays in the process and qualitatively validating many of the same transitions observed by Åysto *et al.* Further measurements by Saastamoinen *et al.* have produced the best-resolution, highest-statistics spectra to date for decay energies $E_p > 500$ keV [3], reporting 16 unique ^{31}Cl β -delayed proton channels. That experiment utilized double-sided silicon strip detectors (DSSSDs) to measure proton decays and a single high-purity germanium (HPGe) crystal to detect β -delayed γ rays.

Saastamoinen *et al.* tentatively reported evidence that some of the β -delayed protons from ^{31}Cl decay were populating excited states of ^{30}P , specifically citing the observation of proton- γ coincidences between events in the 1.2-MeV proton group and 1.5-MeV γ rays. However, without a high-efficiency array of HPGe detectors, determining the $^{30}\text{P}^*$ population distribution was not possible, and the $^{31}\text{S}^*$ feedings and proton intensities were reported under the assumption that all β -delayed proton decays populate the ground state of ^{30}P [3, 4]. However, using GADGET, which couples a gaseous Proton Detec-

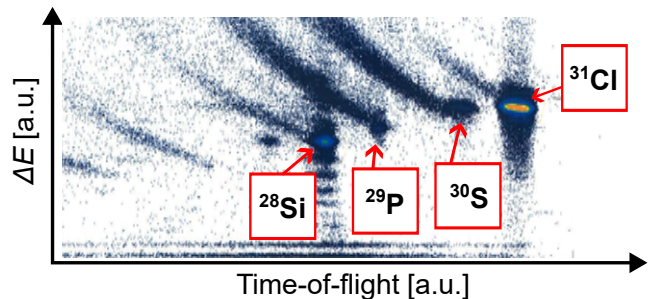


FIG. 1. Particle identification spectrum for the ^{31}Cl cocktail beam. The energy losses ΔE of beam ions are plotted against their time-of-flight as measured between two plastic scintillators in the A1900 Fragment Separator.

tor and the high angular coverage of SeGA [28], we have collected the largest ^{31}Cl β -delayed, proton- γ coincidence dataset to date.

III. NSCL EXPERIMENT

A stable beam of ^{36}Ar was extracted from an electron cyclotron resonance ion source and accelerated to an energy of 150 MeV per nucleon using the NSCL Coupled Cyclotron Facility. At an ion current of 75 pA, this primary beam was impinged on a beryllium fragmentation target, 1645-mg/cm² in thickness, producing a cocktail beam of various nuclides. Using magnetic rigidity and a 150-mg/cm²-thick aluminum wedge, the A1900 fragment separator [29] was optimized for maximal ^{31}Cl beam intensity while minimizing impurities from other nuclear species. The secondary beam was further purified using the Radio Frequency Fragment Separator (RFFS), which utilizes a time-varying electric field synchronized with the cyclotron RF [30]. The phase of this oscillating field pulse was tuned to selectively deflect the ions of interest through the narrow exit slits, while simultaneously filtering out undesirable contaminants. Upon exiting the RFFS, a 65% pure beam of ^{31}Cl was delivered to the experimental vault at an average rate of ≈ 6000 pps. In decreasing order of intensity, the main beam contaminants were the isotones ^{28}Si , ^{30}S , and ^{29}P , as shown in Fig. 1. Fortunately, none of these species are β -delayed charged-particle emitters that would contribute to background in our proton spectrum.

A six-faced, cross-shaped vacuum chamber was connected to the end of the radioactive beam line. This diagnostic cross housed a retractable 300- μm -thick PIN detector, whose position within the chamber was controlled remotely using a pneumatic drive. Between data production runs, the beam current was attenuated and the silicon diode was inserted into the path of the beam in order to measure the energy loss ΔE of ions passing through the semiconducting material. After collecting PIN data

for ≈ 10 min, the relative peak positions corresponding to the different ions within the ΔE histogram were compared with LISE⁺⁺ calculations of ΔE in $300 \mu\text{m}$ of silicon for all nuclear species present in the secondary beam [31]. In addition to the γ -ray signatures observed in SeGA, this particle identification method consistently verified that ^{31}Cl and ^{28}Si comprised the majority of nuclear fragments delivered during the course of the β -decay measurement.

Before each resuming data production cycle, the PIN detector was retracted from the radioactive beam line such that the unattenuated ions could be implanted in the center of the GADGET setup, thermalizing in a cylindrical volume of 800-Torr P10 gas within the Proton Detector chamber. In order to stop the bulk of the radioactive beam in the middle of the gaseous detector's active region, a rotatable, 0.75-mm-thick degrader foil of highly pure ($> 99\%$) aluminum was used to tune the energy of the incoming ^{31}Cl particles. This energy degrader was positioned in the air gap between the end of the beam line and the entrance aperture to the detector chamber, which is sealed with a thin window of Kapton plastic. The degrader angle was measured using a 360° -protractor and was manually adjusted until the ^{31}Cl distribution was longitudinally centered within GADGET, as shown in Figure 2.

The Proton Detector's principle of operation was based on the AstroBox system developed at Texas A&M University [32]. GADGET's conceptual design, its performance testing, and successful commissioning experiment at NSCL are thoroughly described in Ref. [33]. In short, the calorimetric design of the Proton Detector was built to measure weak, low-energy, β -delayed proton decays with high efficiency and low background from β particles. The slower, more massive charged particle ionize the dense fill gas and stop over short ranges within the Proton Detector's cylindrical active region, while the lighter, faster-moving β particles escape the active region, ionizing very little of the gas in the process. A uniform, 150-V/cm electric field ensures that the drift time for the ionization electrons produced by β -delayed particle radiation is proportional to the distance between the location of the β -decay event and the Proton Detector's anode plane. Under these conditions, the maximum drift time for electrons traversing a distance between the cathode, which supplies the voltage for the drift field, and the detector's amplification region within the Micro-Mesh Gaseous Structure (MICROME GAS) [34] is $\approx 7.5 \mu\text{s}$. This defines a $7.5\text{-}\mu\text{s}$ time window after a γ -ray event is detected by SeGA for a coincident charged-particle event to be observed in the Proton Detector.

For rare isotope beam experiments, GADGET operates in alternating cycles of beam implantation, during which radioactive nuclei accumulate in the gaseous detector chamber, followed by a decay-measurement period, during which beam delivery is turned off, and β -delayed

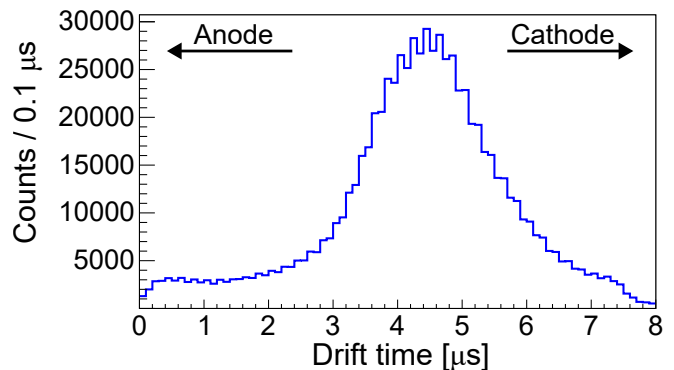


FIG. 2. Drift times of sub-200-keV, β -particle energy depositions detected in coincidence with 2234-keV γ rays. This serves as a rough approximation of the longitudinal distribution for ^{31}Cl β^+ decays throughout the active volume of the Proton Detector.

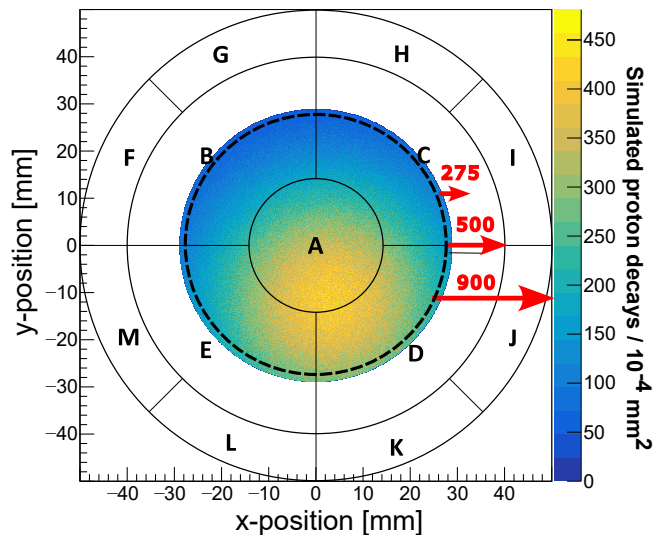


FIG. 3. Reconstructed beam spot representing the transverse distribution of ^{31}Cl ions overlaid on the segmented anode plane. Active detector pads are labeled A-E, and the outer veto pads are labeled F-M. The dashed circle shows the projection of the beam entrance aperture onto the MICROME GAS board. Arrow sizes correspond to the track-lengths of ionization electrons produced by 275-, 500-, and 900-keV proton decays constrained to the $x - y$ plane in an 800-Torr, P10 fill gas, according to the Stopping and Range of Ions in Matter (SRIM) calculator [35].

proton decays are detected by the MICROME GAS. Given its 190-ms half-life [3], a 300-ms implantation period and a 200-ms measurement window were chosen to maximize detection efficiency for ^{31}Cl β -delayed proton decay, while still protecting the MICROME GAS preamplifier during beam implantation. The Proton Detector employs an electronic gating grid of gold-plated copper wires in front of the anode plane. Its applied bias voltage is synchronized with the beam-delivery cycle, such that

strong ionization currents induced by ion implantation are repelled, while weak, low-energy, β -delayed proton decays are still detectable during the 200-ms measurement window.

As depicted in Figure 3, the anode detector plane is segmented into 13 charge-sensitive MICROMEGAS pads, which are responsible for providing gain to the electronic signals produced by β -decay events. The five inner pads are used to measure the full energy and intensity of β -delayed proton decays, while the eight outer pads are used to veto higher-energy protons that would otherwise register cumulatively as a continuum of partial energy depositions in the spectrum. Decay events whose ionization tracks deposit energy in any of the veto pads are rejected from our analysis to reduce continuum background in the β -delayed proton spectrum. The active region of the Proton Detector is contained within a cylindrical volume between the anode and cathode planes, whose radius is defined by the boundary between the inner active pads and the outer veto pads.

The energies and timestamps of events detected by the diagnostic PIN detector, the 13 charge-sensitive MICROMEGAS pads, the central contacts of all 16 SeGA crystals, as well as the switch signal responsible for synchronizing the gating grid with the beam cycle, were collected using two 16-channel PXI digital processor cards and the NSCL Digital Data Acquisition System [36]. The cumulative dataset referenced throughout this article consists of measurements taken over the course of ≈ 86 h of radioactive beam time, with most data production runs lasting ≈ 60 min each.

IV. DATA ANALYSIS

A. γ -ray energy and efficiency calibration

The γ -ray singles spectra were gain-matched on a run-by-run basis using four well-known room-background γ rays from ^{228}Ac , ^{40}K , ^{214}Bi , and ^{208}Tl , with energies of 911, 1461, 1764, and 2615 keV, respectively [37]. A single ^{31}Cl β -delayed γ transition at 6279 keV was also used to extend this calibration to higher energies. In the uncalibrated spectra, these photopeaks were fit using a Gaussian distribution for each SeGA detector. Linear relationships between the Gaussian centroid positions and their corresponding γ energies were determined for 15 of the 16 detectors; a single HPGe crystal exhibited poor energy resolution and was excluded from this analysis.

Enforcing the condition that γ rays must be observed in coincidence with either β^+ or proton events detected by the MICROMEGAS results in the spectrum shown in Figure 4. Gating on Proton Detector events when plotting the γ spectrum not only reduces the amount of room background observed in SeGA, but it also removes γ events originating from ^{31}Cl decays which oc-

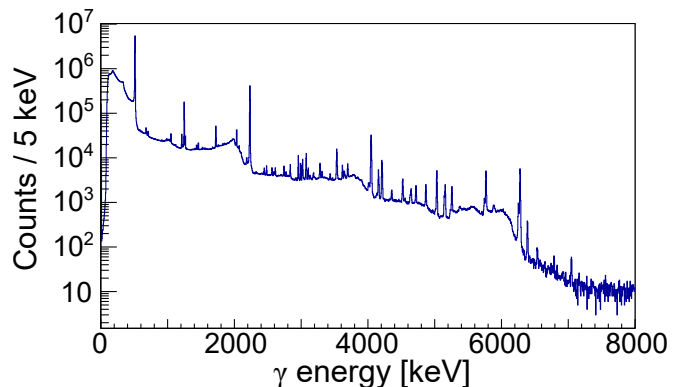


FIG. 4. The ^{31}Cl β -delayed, γ -ray singles spectrum, gated on all coincident charged-particle detections, including β^+ particles. Any γ events recorded in this spectrum must be observed within the same 7.5- μs window as a charged-particle event detected in the Proton Detector.

curred outside the active volume of the ionization chamber or during the beam implantation period when the electronic gating grid prevents signal collection in the MICROMEGAS. This is useful for the purpose of normalization when determining relative decay intensities.

GADGET's efficiency to detect γ rays was determined for energies $E_\gamma \lesssim 7$ MeV. This was achieved by first measuring the number of observed γ -ray transitions across a range of energies. Out of the strongest $^{31}\text{S}^*$ transitions, 12 well-separated photopeaks were fit with an asymmetric Gaussian distribution, while the local background was modeled as either a first- or second-degree polynomial. The exponentially modified Gaussian (EMG) distribution can be written in terms of the complementary error function (erfc) as

$$f(x; \mu, \sigma, \lambda) = \frac{N\lambda}{2} \exp \left[\frac{\lambda}{2} (\lambda\sigma^2 \pm 2\mu \mp 2x) \right] \times \text{erfc} \left(\frac{\lambda\sigma^2 \pm \mu \mp x}{\sqrt{2}\sigma} \right), \quad (1)$$

where μ and σ correspond to the centroid and width of the function's Gaussian component, respectively, while λ determines the size of the asymmetry. The plus-minus symbols imply that this response function can account for skew in both directions: a high-energy tail in the case of the Proton Detector due to β^+ summing and a low-energy tail in the case of SeGA due to incomplete charge collection. The normalization factor N is the definite integral of the function, which determines the total number of recorded decay events in each peak.

Since Ref. [6] is the most complete study of $^{31}\text{Cl}(\beta\gamma)^{31}\text{S}$ to date, we adopt its β -decay feedings I_β , which were used to deduce the corresponding γ intensities I_γ . However, the originally reported I_γ values contained some minor internal inconsistencies and have since

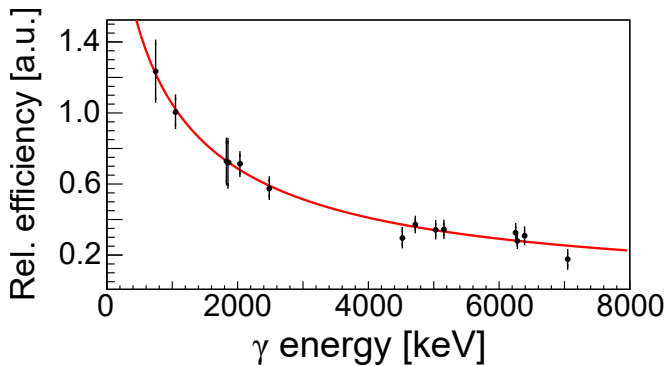


FIG. 5. Relative detection efficiency plot for SeGA as a function of E_γ .

been corrected in the evaluated literature [38]. Figure 5 shows SeGA’s relative efficiency for γ -ray detection as a function of energy, fit with a power-law function for the purpose of interpolation.

To determine the probability of detecting a γ -ray event with energy $0.6 < E_\gamma < 7.1$ MeV, the fit in Figure 5 was scaled to match the absolute detection efficiencies of the two strongest γ transitions in the spectrum, which were independently determined. Normalizing detection efficiency at specific energies is possible if two quantities are well known: (1) the observed number of incoming transitions γ_{in} for a given level, as determined by fitting the γ -ray singles spectrum in Figure 4 and (2) the number of outgoing transitions γ_{out} detected in coincidence with γ_{in} ; see Figure 6 for example. Assuming there are no other outgoing γ transitions from this level, we can express the probability of detecting γ_{out} as the ratio

$$\epsilon(\gamma_{\text{out}}) = \frac{\text{Observed } \gamma_{\text{in}}\text{-}\gamma_{\text{out}} \text{ coincidences}}{\text{Observed } \gamma_{\text{in}} \text{ singles}}, \quad (2)$$

which was scaled by a factor of 15/14 to account for possible coincidence photons summing their combined energy in a single SeGA detector. This relationship was used to determine the absolute detection efficiencies of 4.5(5)% and 2.7(6)% for the 1248- and 2234-keV γ rays, respectively. These γ decays correspond to ground-state transitions from the two lowest-lying excited states in ^{31}S . The fact that these levels are populated via several intense γ decays from more highly excited states allowed us to verify our method for determining absolute detection efficiency using multiple incoming γ transitions.

We do not find evidence for additional $^{31}\text{S}^*$ γ transitions beyond what has been reported in Ref. [6]. However, a detailed analysis of proton- γ coincidence data reveals many previously unobserved β -delayed proton decays, most of which populate excited states of ^{30}P . Knowing the absolute SeGA efficiency over a wide range of γ energies is useful for determining the intensity of weak, β -delayed proton decays detected in coincidence with $^{30}\text{P}^*$

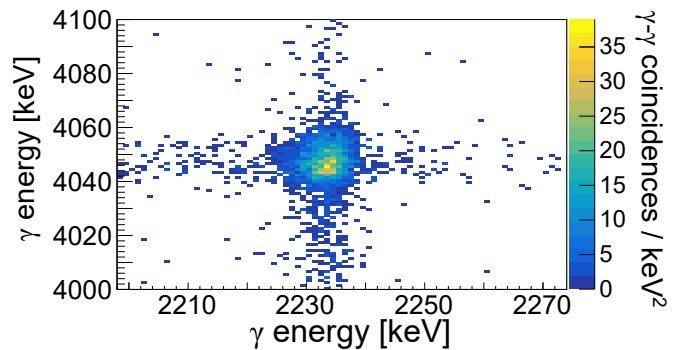


FIG. 6. Observed γ - γ coincidences between the 4045- and 2234-keV transitions from $^{31}\text{S}^*$ decay. Employing Equation 2, this pair of transitions was used to normalize the absolute γ -ray detection efficiency at 2234 keV for GADGET.

γ rays.

B. Proton- γ coincidences and proton energy calibration

As with the γ -ray data, the proton spectra were gain-matched on a run-by-run basis for each of the five inner MICROMEGAS pads. However, because there were significantly fewer proton counts per run than γ -ray events, Proton Detector data acquired over shorter runs ($\lesssim 60$ min) were combined with events from longer, consecutive runs. The limited statistics also meant that this linear gain-matching procedure relied on the positions of the only two peaks that could be consistently fit with Gaussian distributions in the spectra of all active pads. These features correspond to the two strongest ^{31}Cl β -delayed proton transitions, with decay energies of 0.8 and 1.0 MeV [3, 4, 39].

The cumulative singles spectra are shown in the bottom panel of Figure 7 for all non-vetoed, β -delayed proton decay events observed in the active region of the Proton Detector and for events observed in only a single detector pad. At the lowest energies, the spectrum is dominated by an exponential background of β^+ particles. Just below 300 keV, we observe a small proton peak corresponding to the decay of a crucial $\ell = 0$ resonance for the $^{30}\text{P}(p, \gamma)^{31}\text{S}$ reaction in oxygen-neon (ONe) novae, which is the subject of Ref. [7]. In the energy region $300 < E_p < 700$ keV, the relatively flat background results from a “wall effect,” whereby higher-energy protons near the upstream or downstream end of the detector chamber deposit some, but not all, of their energy into ionizing the fill gas before implanting in the cathode or anode, respectively.

For center-of-mass energies $E_p(\text{c.m.}) > 800$ keV, we observe almost all of the same ^{31}Cl β -delayed proton decay peaks previously reported in literature [2–4, 24–27]. Some of these previous measurements had better

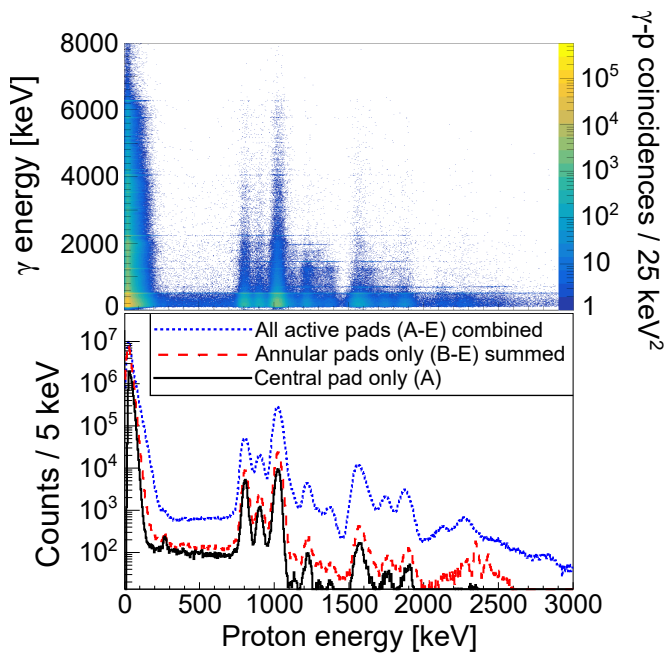


FIG. 7. (Top) All observed coincidences between γ rays and charged-particle decays, including β -delayed protons. (Bottom) Proton Detector singles spectra for all non-vetoed events measured in the active region [dotted gray (violet online)], the summed statistics from each of the four annular pads' individual spectra [dashed gray (red online)], and decay events only detected in the central MICROMEGAS pad [solid black].

energy resolution and detection efficiency at higher energies [3, 4]. However, due to a lack of high-statistics, proton- γ coincidence information, these β -delayed proton transitions were assumed to directly populate the ground state of ^{30}P [39]. The γ -tagging capabilities of GADGET reveal that certain features resembling individual peaks within the proton singles spectra actually contain multiple contributions from various β -delayed proton transitions feeding different ^{30}P levels. This is illustrated in Figure 8, which plots only the γ -ray events detected in coincidence with proton decays for which $1.2 < E_p(\text{c.m.}) < 1.3$ MeV. In this proton-gated γ spectrum, there are six photopeaks that clearly stand out from the background, whose energies correspond to all known γ rays emitted in the decay of the first four excited states of ^{30}P [40–43].

Conversely, by placing coincidence gates on all $^{30}\text{P}^*$ γ rays, we are able to plot a unique spectrum for each final state populated by β -delayed proton decay in the daughter nucleus. A careful background subtraction procedure was performed in order to account for both the “accidental” contribution of proton transitions in random coincidence with $^{30}\text{P}^*$ γ rays, as well as the “real” contribution from non-random coincidences between protons populating $^{30}\text{P}^*$ states and the γ rays that fall within the low-energy tail of the corresponding γ transition’s photopeak. This was achieved by modeling the normalized singles spectra as protons in coincidence with the γ -ray

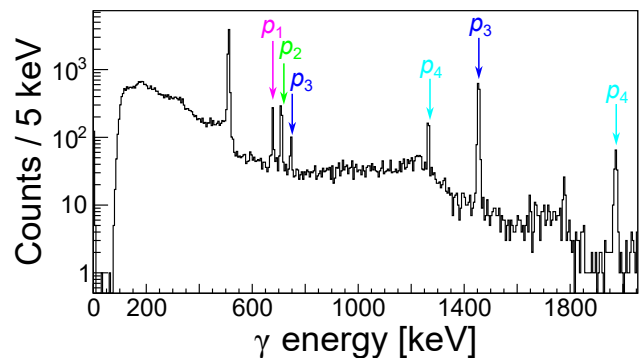


FIG. 8. Energy spectrum for γ rays detected in coincidence with proton decays in the energy region $1.2 < E_p(\text{c.m.}) < 1.3$ MeV. The photopeaks labeled p_1 , p_2 , p_3 , and p_4 correspond to transitions associated with the γ decay of the 677-, 709-, 1454-, and 1973-keV excited states of ^{30}P , respectively.

background region slightly higher in energy than the $^{30}\text{P}^*$ photopeak of interest, whose energy range was varied to quantify the uncertainties associated with both true and random coincidences.

This analysis procedure results in the γ -gated, background-subtracted proton spectra depicted in Figure 9, which clearly shows new transitions populating the 677-, 709-, 1454-, and 1973-keV levels. Many of these previously unidentified, β -delayed proton decays are quite weak and would otherwise be obscured in the ungated singles spectrum. In energy regions where there are strong ground-state (p_0) transitions, such as around 1.0 MeV, the uncertainties of the bin-by-bin subtraction between the photopeak-gated and background-gated histograms are relatively large, making it difficult to identify particularly weak β -delayed proton decays in this energy regime. Nevertheless, our findings showcase GADGET’s potential as a powerful tool for nuclear spectroscopy, resulting from its complementary subsystems, with sensitivity to both charged-particle and γ -ray emission.

The identification of many new β -delayed proton decays in Figure 9 allows us to refine the energy calibration from Ref. [7] and extend it to higher proton-decay energies. First, we adopted the evaluated level energies from the latest version of the $A = 31$ Nuclear Data Sheets for the three strongest proton-emitting states populated in ^{31}Cl β^+ decay at 6936(2), 7037(2), and 7157.5(11) keV [38]. Utilizing the relationship

$$E_{x_i}(^{31}\text{S}) = S_p + E_p(\text{c.m.}) + E_{x_f}(^{30}\text{P}), \quad (3)$$

where $E_{x_i}(^{31}\text{S})$ is the initial excitation energy, $S_p = 6130.65(24)$ is the ^{31}S proton separation energy [44], and $E_{x_f}(^{30}\text{P})$ is the excitation energy of the final ^{30}P state, we computed the center-of-mass decay energies of our initial calibration points $E_p(\text{c.m.})$: 805(2), 906(2)

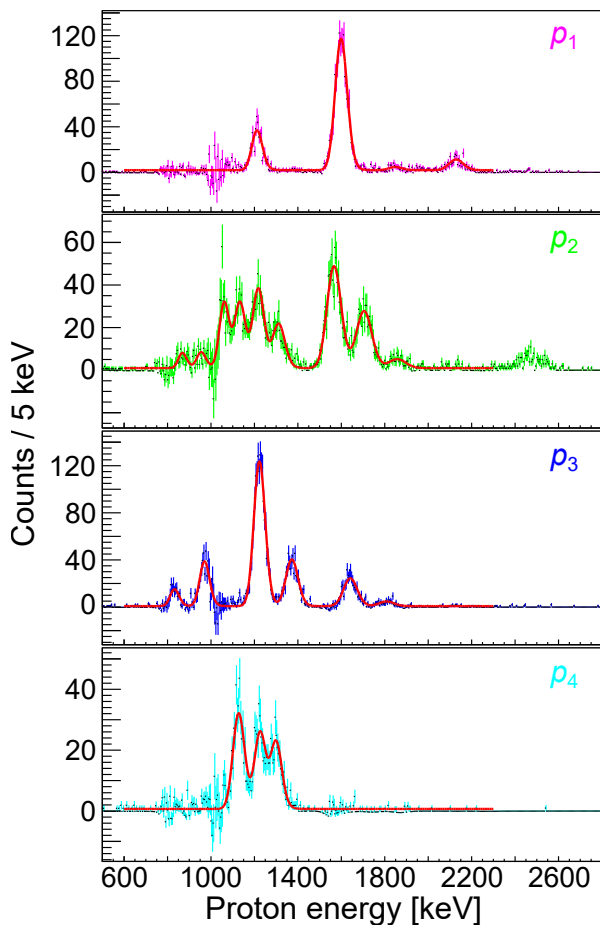


FIG. 9. The γ -gated proton spectra after background subtraction. Each panel shows ^{31}Cl β -delayed protons populating the first [p_1 (magenta online)], second [p_2 , (green online)] third [p_3 (blue online)], and fourth [p_4 (cyan online)] excited states of ^{30}P . Fits [solid gray (red online)] are superimposed.

and 1026.9(11) keV. By fitting the corresponding proton peaks in the combined singles spectrum of Figure 7 and determining a linear relationship between peak position and decay energy, we defined a local calibration with a 3-keV uncertainty band in the region $0.8 < E_p < 1.0$ MeV.

In Figure 9, we identified several weak, β -delayed protons within our valid calibration region, including one particular decay at $E_{p_3} = 834(3)$ keV, which populates the 1454-keV level of ^{30}P . Again using Equation 3, we determined the ^{31}S excitation energy of the corresponding proton-unbound state to be $E_{x_i} = 8418(3)$ keV. This is quite close to a previously observed level, whose evaluated excitation energy $E_{x_i} = 8424(3)$ keV [38] is a weighted average of the results from Refs. [4, 11, 21]. Thus, we consider the present work to be an independent measurement of this level and use our 8418-keV excitation energy for the purpose of our calibration.

Further analysis revealed that this 8418-keV level is re-

sponsible for three additional proton peaks observed in our spectra, one of which is the 2.3-MeV ground-state decay previously reported by Saastamoinen *et al.* The other two β -delayed proton transitions through this state occur at decay energies near 1.6 MeV and populate the 677- and 709-keV excited states of ^{30}P . Thus, four well-known ^{31}S levels can be used to constrain seven proton-energy calibration points across the region $0.8 < E_p < 2.3$ MeV, making linear extrapolation to lower decay energies more robust. Applying this more precise calibration to evaluate the energy of the astrophysically relevant resonance in Ref. [7], we report a revised value of $E_{p_0} = 258(4)$ keV with reduced uncertainty, bringing us into agreement with Bennett *et al.* at the level of a single standard deviation [5, 6].

The energies of all ^{31}Cl β -delayed proton decays observed in NSCL Experiment 17024 are provided in Table I. Equation 3 allowed us to use these calibrated proton-decay energies to compute the initial excitation energies, which are also tabulated. In other cases where multiple proton transitions are attributed to the decay of the same ^{31}S level, a weighted average is used for the excitation energy.

C. Proton intensities and efficiency simulations

The high-statistics, proton- γ coincidence information obtained with GADGET allows us to place stricter constraints when analyzing the cumulative proton energy spectrum across all active detector pads shown in Figure 7. Four energy regimes, each on the order of several hundred keV in width, were fit using multiple EMG distributions to model proton peaks across the entire spectrum. The local backgrounds of these fits were modeled as linear, and the detector response function describing the peak shape was constrained to vary smoothly with decay energy, under the assumption that all resonances are intrinsically narrow; no evidence of broad resonances was identified.

Initially, the coarse features of the cumulative proton singles spectrum were fit under the assumption that each visible peak corresponds to a unique p_0 decay, allowing the Gaussian centroid and integral of the distribution to vary freely in order to estimate the total number of proton counts. Then, the contributions from weaker excited-state transitions identified in Figure 9 were iteratively added to these fits. After correcting for SeGA's γ efficiency, the positions and intensities of these smaller peaks were fixed in the cumulative spectrum. In energy regimes where p_1 , p_2 , p_3 , and p_4 transitions are visible in the proton singles spectrum from Figure 7, the number of decays determined by fitting the singles peaks agrees with the integrals of the fits from the γ -gated spectra in Figure 9 to within a factor of $\lesssim 2$ when accounting for γ -ray detection efficiency.

In order to report normalized β -delayed proton intensities I_p and plot $\Sigma B(\text{GT})$ as a function of ^{31}S excitation energy, the Proton Detector efficiency must be quantified. Detailed simulations using the GEometry ANd Tracking (GEANT4) framework were performed during the design, testing, and commissioning phases of GADGET development [33]. These Monte Carlo simulations were performed by randomly sampling the positions of decay events from an initial ^{31}Cl beam distribution and counting the number of proton tracks that were contained within the active region of the Proton Detector. The longitudinal component of this beam distribution was modeled using the ionization drift times plotted in Figure 2, while the transverse component was defined by the beam spot in Figure 3. Using the multiplicity of total counts detected in each of the five inner MICROMEAS pads, a χ^2 -minimization procedure was used to determine the position and width of the Gaussian beam spot to within ± 6 mm.

Since performing this experiment at NSCL in November 2018, the Proton Detector has undergone an upgrade, allowing the GADGET II system to operate as a time projection chamber (TPC) at the Facility for Rare Isotope Beams (FRIB) [45]. In the process of this upgrade, it was discovered that the degree to which electrons diffuse in P10 gas could have a larger effect on the final detection efficiency than originally assumed. Decay protons lose most of their kinetic energy in the Proton Detector through ionizing the gaseous medium, and the total number of electrons liberated in ionization depends on both the energy loss in the gas and the average energy required to create a single electron-ion pair for a given gas mixture. As the ionization electrons drift through the chamber under the influence of a uniform electric field, they diffuse transversely according to the relation $\sigma(t) = \sqrt{4D_e t}$ until they reach the amplification region of the MICROMEAS [46]. For an 800-Torr P10 gas mixture and a 150-V/cm drift field, the electron diffusion constant was calculated to be $D_e = 9.12(27) \times 10^3$ cm²/s using the MAGBOLTZ program [47].

To determine the size of this effect on the detection efficiency, we developed a Simplified Geometric Monte Carlo (SGMC) model that was able to reproduce the more detailed GEANT4 results, which do not account for electron diffusion, to within 3% up to 1.5-MeV proton energies. Using the same initial ^{31}Cl beam spot and longitudinal profile, the SGMC model randomly samples the starting coordinates of a decay event from the reconstructed beam distribution, assumes proton radiation is emitted isotropically, and uses stopping powers calculated in SRIM to determine the final position of the thermalized proton within the gaseous detector medium [35]. If a proton's full ionization track was contained within the active volume, we considered this a detected event; otherwise, this decay event would trigger the veto condition. In order to incorporate the effect of electron

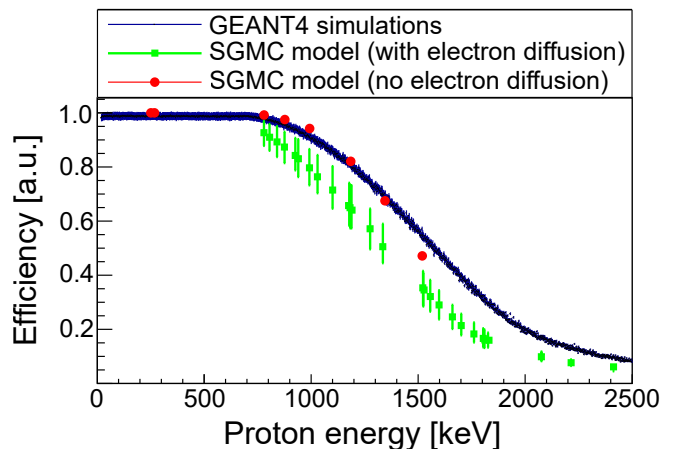


FIG. 10. Proton Detector efficiencies comparing GEANT4 simulations with no electron diffusion [solid black (blue online)] to the SGMC model, both with [square data markers (green online)] and without [circular data markers (red online)] the radial electron diffusion effect.

diffusion into this model, for every 10- μm step along the length of the proton track, we randomly sampled the positions of n_{e^-} ionization electrons from a two-dimensional Gaussian distribution, whose size depends on the drift time of a randomly selected β -decay event, and where n_{e^-} is proportional to the proton's ΔE over that 10- μm distance. Ultimately, we used the SGMC model to evaluate GADGET's efficiency across all relevant proton energies. Figure 10 compares simulation results with and without electron diffusion to the GEANT4 model.

Many iterations of the SGMC calculations were performed over a variety of experimental conditions in order to rigorously investigate these systematic effects on the Proton Detector efficiency. One of the largest sources of uncertainty in our efficiency model was the initial beam spot distribution. This uncertainty arises from both the diffusion of thermalized beam particles via Brownian motion, as well as the χ^2 -minimization procedure used to determine the parameters of the Gaussian distribution, ultimately resulting in a 2–5% uncertainty on the detection efficiency of a 1.0-MeV proton. Setting the simulation's charge deposition threshold in terms of n_{e^-} for proton event detection was also a source of systematic uncertainty in our model. This is because all MICROMEAS pads have slightly different gains, resulting in thresholds spanning 5–20 keV, which changes the number of ionization electrons required to register an event or trigger the veto condition. This triggering threshold leads to a 3–4% uncertainty in the 1.0-MeV proton detection efficiency. Smaller effects ($\lesssim 1\%$) on the final error bars can be attributed to uncertainties in the SRIM model [35], the electron diffusion constant as calculated by MAGBOLTZ [47], and the electric field distortions produced by slowly drifting positive ions generated by beam particles implanted at the end of the beam-delivery cycle and

near the beginning of the decay-measurement period.

The relative intensities $I_p(\text{rel})$ of all observed transitions along with their corresponding uncertainties are tabulated in Table I. Just as in Ref. [7], the present β -delayed proton intensities were normalized relative to the 1.0-MeV decay intensity $I_p(\text{abs}) = 1.31(2)\%$ adopted from literature [3, 4, 39]. After refining GADGET's proton-detection efficiency model with more detailed numerical simulations, we report $I_p(\text{abs}) = 9.0(10) \times 10^{-6}$ for the 258-keV resonance of interest. Thus, the corresponding proton branching ratio and resonance strength are $\Gamma_p/\Gamma = 2.4(3) \times 10^{-4}$ and $\omega\gamma = 77(45) \mu\text{eV}$, respectively. These revised numbers supersede the previously reported values, and any discrepancies have a negligible effect on the astrophysical conclusions.

Table I shows that several ^{31}S excited states populated in ^{31}Cl decay are located above the α emission threshold at $S_\alpha = 9082.935(22)$ keV [44], but the calorimetric nature of GADGET prevents distinguishing α particles from protons. With the recent TPC upgrade to the GADGET II system [45], discriminating between ^{31}Cl β -delayed proton and α events is possible. However, since the Coulomb barrier suppresses significant α emission for charged-particle decays $\lesssim 10$ MeV, we assume all β -delayed particles observed in our spectra are the result of proton decays.

V. RESULTS AND DISCUSSION

In total, up to 29 unique β -delayed proton transitions have been observed in NSCL Experiment 17024, of which 11 have been reported in prior ^{31}Cl β -decay studies [2–4, 24–27, 51]. Although all previously observed decays were reported to populate the ground state of ^{30}P , as many as 20 of the present transitions are now assigned to one of the four lowest-lying excited states of ^{30}P , as illustrated in Figure 11. Here we provide a brief discussion of ^{31}S level assignments, as well as the extracted GT strength distribution compared to prior experiments and theory.

A. Excitation energies for ^{31}S levels

Almost all of the ^{31}S excitation energies determined in this work agree with the most recently evaluated nuclear level assignments to within two standard deviations [38]. Thus, the vast majority of states populated in ^{31}Cl β^+ decay have already been observed in previous experiments using various techniques and channels. Nevertheless, there are several cases where the present excitation energies disagree with prior measurements by more than 10 keV.

One such exception is the ^{31}S level in the 7.8-MeV region, which was reported in Refs. [3, 11, 14, 55]. Our

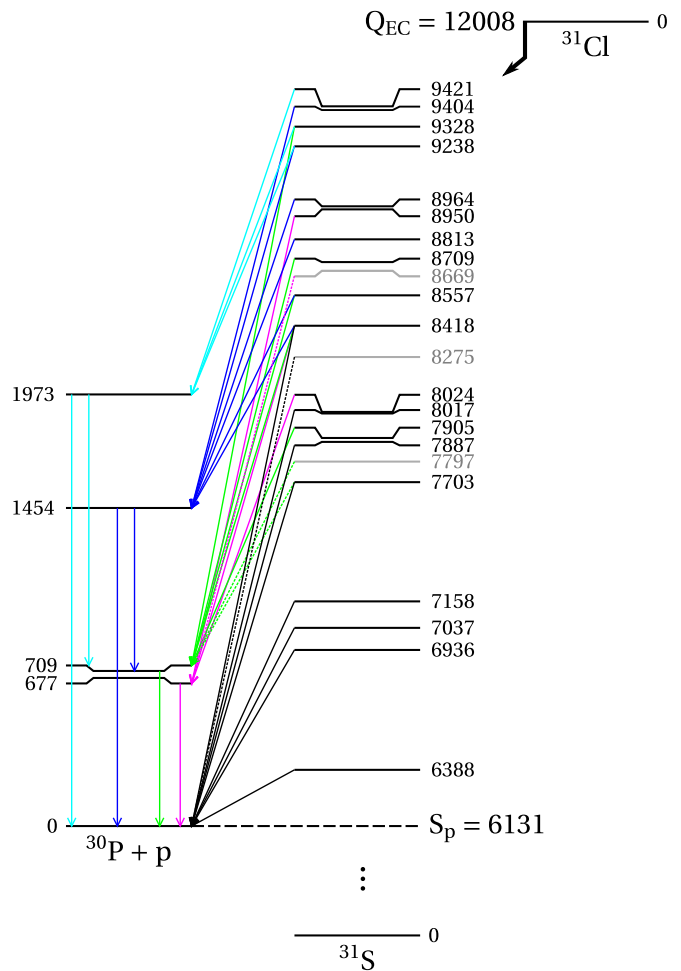


FIG. 11. The $^{31}\text{Cl}(\beta p \gamma)^{30}\text{P}$ decay scheme. Transitions from proton-unbound levels in ^{31}S to excited states in ^{30}P are shown as gray arrows [magenta (p_1), green (p_2), blue (p_3), or cyan (p_4) online], while ground-state (p_0) transitions are represented by black arrows. The ^{30}P γ -ray transitions are color-coded to match the β -delayed proton decays populating their respective excited states. Tentative transitions' arrows are dashed, and tentative ^{31}S levels are shown in gray. All energies are reported in units of keV.

tentative observation of this level depends on a very weak 958-keV proton decay, which may populate the 709-keV excited state of ^{30}P . However, due to the high statistics of the nearby 1.0-MeV p_0 peak, the uncertainties associated with background subtraction in this region of the energy spectrum are quite large. For this reason, we cannot definitively claim this as evidence of a new ^{31}S level or a unique β -delayed proton transition.

Another similar example of background subtraction's effect on the uncertainties of γ -gated protons peaks is the tentative observation of a weak 1862-keV proton transition to the 677-keV excited state of ^{30}P . We do find evidence of a much stronger β -delayed proton transition populating the 709-keV state, which has approximately the same decay energy. Due to the first and second ex-

$E_{x_i}({}^{31}\text{S})$ [keV]		J^π present	$I_\beta(\text{abs})$ [%]	$\log(ft)$ present	$E_{x_f}({}^{30}\text{P})$ [keV]	$E_p(\text{c.m.})$ [keV]		$I_p(\text{rel})$ [%]	
[38]	present					[3]	present	[3]	present
6390.46(16)	6388(4)	$3/2^+$ [5]	3.38(18) [5]	4.11(2)	0	—	258(4)	—	0.069(5)
6936(2)	—	$1/2^+, 3/2^+, 5/2^+$	0.20(2)	5.09(4)	0	806(2)	805(2)*	20.4(2)	$15.4^{+0.7}_{-0.8}$
7037(2)	—	$5/2^+$ [22]	0.087(9)	$5.40^{+0.05}_{-0.04}$	0	906(2)	906(2)*	12.4(2)	6.6(4)
7157.5(11)	—	$3/2^+, 5/2^+$ [21, 22]	1.31(2) [3]	4.162(7)	0	1026(2)	1026.9(11)*	100(4)	100^{+9}_{-8}
7699(3)	7703(3)	$1/2^+, 3/2^+, 5/2^+$	0.14(3)	$4.83^{+0.10}_{-0.08}$	708.70(7) 0	—	870(18) 1571(3) 1572(3)	—	< 0.05 21.0(4) 10.8(20)
7774(3)	7797(12)		< 0.0005	> 7.19	708.70(7)	—	958(12)	—	< 0.05
7895(2)	7887(3)	$1/2^+, 3/2^+, 5/2^+$	0.038(8)	5.29(9)	0	1763(3)	1756(3)	6.4(2)	$2.9^{+0.6}_{-0.5}$
7907(2)	7905(8)	$1/2^+$ [10]	0.0027(7)	$6.43^{+0.13}_{-0.11}$	708.70(7)	—	1065(8)	—	0.20(5)
8015(3)	8017(3)	$1/2^+, 3/2^+, 5/2^+$	0.09(2)	$4.83^{+0.09}_{-0.08}$	0	1891(3)	1887(3)	10.9(2)	$6.9^{+1.3}_{-1.1}$
8022(3)	8024(2)	$1/2, 3/2, 5/2$	0.0034(7)	$6.25^{+0.10}_{-0.09}$	677.11(10)	—	1217(2)	—	0.26(5)
8268(10)	8275(4)		< 0.008	> 5.70	0	2139(17)	2145(4)	1.3(1)	< 0.6
8424(3)	8418(3)	$1/2^+, 3/2^+, 5/2^+$	0.09(1)	$4.53^{+0.05}_{-0.06}$	1454.28(5) 708.70(7) 677.01(3) 0	—	833(3)* 1579(3)* 1610(3)* 2298(3) 2287(5)*	—	0.10(1) 1.0(2) $2.2^{+0.5}_{-0.4}$ $4.0^{+0.8}_{-0.6}$
8563(2)	8557(2)	$1/2^+, 3/2^+, 5/2^+$	0.015(3)	$5.21^{+0.08}_{-0.07}$	1454.28(5) 708.70(7)	—	973(2) 1715(4)	—	0.33(5) 0.8(2)
8702(17)	8669(8) 8709(7)	$(1/2^+, 3/2^+, 5/2^+)$	< 0.019 0.0028(8)	> 6.04 $5.82^{+0.13}_{-0.11}$	677.11(10) 708.70(7)	—	1862(8) 1869(7)	—	< 0.14 $0.22^{+0.06}_{-0.05}$
8815(3)	8813(2)	$1/2^+, 3/2^+, 5/2^+$	0.019(4)	4.92(9)	1454.28(5)	1225(3)	1228(2)	2.7(1)	$1.4^{+0.3}_{-0.2}$
8973(4)	8950(5) 8964(2)	$1/2^+, 3/2^+, 5/2^+$ $1/2^+, 3/2^+, 5/2^+$	0.010(8) 0.009(3)	$5.1^{+0.6}_{-0.2}$ $5.10^{+0.13}_{-0.11}$	677.11(10) 1454.28(5)	—	2143(5) 1390(17) 1379(2)	—	0.7(6) 1.3(12) 0.7(2)
9226(25)	9238(2)	$1/2^+, 3/2^+, 5/2^+$	0.016(3)	$4.58^{+0.09}_{-0.07}$	1973.34(8) 1454.28(5)	—	1137(4) 1647(17) 1651(3)	—	$0.38^{+0.10}_{-0.09}$ 1.4(2) 0.8(2)
9332(30)	9328(5)	$1/2^+, 3/2^+, 5/2^+$	0.017(5)	$4.44^{+0.13}_{-0.10}$	1973.34(8) 708.70(7)	—	1223(5) 2489(8)	—	0.31(6) 1.0(3)
9423(7)	9404(6) 9421(8)	$1/2^+, 3/2^+, 5/2^+$ $3/2^+, 5/2^+$ [10]	0.003(1) 0.007(4)	$5.08^{+0.13}_{-0.11}$ $4.7^{+0.3}_{-0.2}$	1454.28(5) 1973.34(8)	—	1819(6) 1317(8)	—	$0.25^{+0.07}_{-0.06}$ 0.6(3)

TABLE I. Comprehensive results from the ${}^{31}\text{Cl}(\beta p \gamma){}^{30}\text{P}$ measurement. At present, initial excitation energies $E_{x_i}({}^{31}\text{S})$ and center-of-mass decay energies $E_p(\text{c.m.})$ are compared to the nearest nuclear levels evaluated in literature and previously measured β -delayed proton energies, respectively. Proton-decay energies denoted by an asterisk (*) were used for energy calibration. When available, established spin-parity assignments are adopted from literature on the basis of symmetry arguments from the ${}^{31}\text{P}$ mirror nucleus [5] and angular distribution data from single-nucleon transfer reaction measurements [10, 21, 22]. Otherwise, J^π values are deduced from rules outlined in Refs. [48, 49] for β decay; tentative levels where only $\log(ft)$ lower limits are reported receive no such assignments. The $\log(ft)$ values of ${}^{31}\text{S}$ states were calculated using the RADIATIONREPORT software [50], as part of the Evaluated Nuclear Structure Data File (ENSDF) Analysis and Utility Programs. The β -feeding intensity $I_\beta(\text{abs})$ for each state represents the probability of direct ${}^{31}\text{S}$ -level population from a single ${}^{31}\text{Cl}$ β^+ decay or electron capture. Most of the β^+ feeding to the 6390-keV excited state is observed through subsequent γ -ray emission [5, 6], and proton-decay intensities $I_p(\text{rel})$ are normalized relative to the intensity of the 1.0-MeV proton decay reported in Ref. [3, 4, 39]. The final excitation energies $E_{x_f}({}^{30}\text{P})$ for levels populated by ${}^{31}\text{Cl}(\beta p)$ are also tabulated.

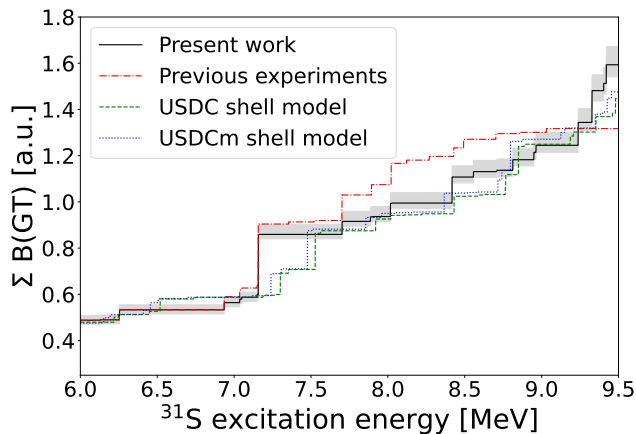


FIG. 12. The cumulative GT strength distribution for ^{31}S proton-unbound states $6.0 < E_{x_i} < 9.5$ MeV. The present experimental evaluation [solid black] is compared to prior measurements [dash-dotted gray (red online)] from Refs. [3, 4], as well as to shell-model theory calculations using the USDC and USDCm Hamiltonians [52]. The gray uncertainty band was determined using propagation of errors for the $\log(ft)$ values in Table I and constants from Refs. [53, 54] in Equation 4.

cited states' close energetic proximity, it is likely that the 1862-keV protons appearing in the p_1 spectrum of Figure 9 are actually in coincidence with the low-energy tail of the 709-keV photopeak.

However, there is evidence for the existence of two previously unobserved ^{31}S levels. We measured a weak 1819-keV transition to the third excited state of ^{30}P , which suggests the existence of a ^{31}S level at $E_{x_i} = 9404(6)$ keV. We also observed a much stronger 2143-keV, β -delayed proton transition to the first excited state of ^{30}P , which implies an initial excitation energy of $E_{x_i} = 8950(5)$ keV. This is sufficiently far removed from the 8964-keV level we observed to decay via 1379-keV proton emission, which we consider to be in rough agreement with previous measurements [3, 11, 21].

The present work has also identified the existence of a 2.1-MeV p_1 transition, which may be the same 2.1-MeV protons reported by Saastamoinen *et al.* as a p_0 decay. Due to the relatively large statistical and systematic uncertainties associated with fitting the spectrum at energies > 2 MeV, it is possible to model the 2.1-MeV peak in the ungated singles spectrum as having contributions from both ground-state and excited-state proton transitions. However, the simpler explanation is that the 2.1-MeV p_0 transition does not exist. Thus, our population of the ^{31}S level in the 8275-keV region is considered tentative. All other excitation energies reported at present should be interpreted as independent measurements of previously observed levels.

B. Comparing theory to experiment

Comparing the present work with data from the best previous ^{31}Cl β -delayed proton measurement, we have identified 11 of the same peaks observed by Saastamoinen *et al.*, and our relative proton-decay intensities agree within a factor of $\lesssim 2$. In all but one case, the present intensities are lower than those reported in Ref. [3, 39], the latter of which sum to a total absolute intensity of $I_{\beta p} = 2.4(2)\%$. Summing the contributions of all observed protons in the present measurement results in a total ^{31}Cl β -delayed proton-decay intensity of $I_{\beta p} = 2.08(5)\%$, agreeing within 1.5 standard deviations of prior experimental work.

The discrepancies between the present and previous measurements are visualized in Figure 12 when plotting the cumulative sum of the experimental $B(\text{GT})$. The GT values are evaluated for each ^{31}S level using the expression

$$B(\text{GT}) = \frac{K/g_V^2}{ft(g_A/g_V)^2}, \quad (4)$$

where $K/g_V^2 = 6144.48(370)$ s and $g_A/g_V = -1.2753(13)$, according to Refs. [53, 54], respectively. These calculations ignore the negligible GT contribution to the predominantly $T = 3/2$, 6279-keV isobaric analog state (IAS), for which proton decay is isospin forbidden. They also neglect the mostly $T = 1/2$, proton-emitting level at 6388 keV, whose β feeding is enhanced by the Fermi interaction due to isospin mixing with the IAS [5]. We compare our experimental evaluation to universal sd -shell model calculations using the isospin-breaking Hamiltonians: USDC and USDCm [52]. The theoretical results plotted in Figure 12 adopt a quenching factor of $q_{\text{GT}} = 0.764$ from Table III in Ref. [56]. Our findings are in better agreement with shell-model theory than previous work for excitation energies $7.5 < E_{x_i} < 9.5$ MeV. This results from the β -feeding intensities spreading out over a larger range of excitation energies, as opposed to being concentrated within a smaller number of proton-unbound levels relatively close to the ^{31}S proton threshold, which were assumed to decay to the ground state of ^{30}P .

C. Future considerations

The current experimental setup was designed to measure small proton branching ratios of low-energy resonances that dominate the $^{30}\text{P}(p, \gamma)^{31}\text{S}$ reaction rate during the thermonuclear runaway event in ONe novae. This required high-efficiency detection of low-energy, β -delayed proton decays with minimal β^+ background. In order to extract more information on ^{31}S levels $E_{x_i} >$

9.5 MeV, the pressure of the Proton Detector’s fill gas could be increased to improve detection efficiency for higher decay energies at the expense of larger β^+ backgrounds and degraded energy resolution. Still, GADGET II could be utilized to distinguish between β -delayed proton and α decays [45]. Alternatively, a $\Delta E - E$ silicon telescope could be deployed in tandem with a high-efficiency HPGe array to measure higher-energy, β -delayed charged-particle decays in coincidence with $^{30}\text{P}^*$ γ rays. Although low-energy α particles would struggle to penetrate through the thin ΔE detector, they could be identified by vetoing events that reach the thicker E detector. Employing this technique would improve both energy resolution and detection efficiency for charged-particle energies $E_p > 1.0$ MeV.

VI. CONCLUSIONS

This study provides a first look at the $^{31}\text{Cl}(\beta p \gamma)^{30}\text{P}$ decay sequence. Previous measurements of ^{31}Cl β^+ decay only provided substantial information on the proton singles or $^{31}\text{S}^*$ γ -ray spectra. The results obtained from NSCL Experiment 17024 combine high-statistics, proton- γ coincidence data to reveal many previously unobserved β -delayed proton transitions to excited states in the ^{30}P daughter nucleus. Our findings demonstrate an example of “proton pandemonium,” and the techniques discussed in the present work are valuable for making accurate comparisons to theoretical models.

Furthermore, this article demonstrates the technical prowess of the GADGET system for measuring weak, low-energy, β -delayed charged-particle decays in coincidence with high-efficiency, γ -ray detection capabilities and good energy resolution. GADGET has already been successfully utilized in a several scientific experiments [7, 57, 58] and is a useful instrument for studying resonances involved in charged-particle capture on both ground and excited states of unstable nuclei in astrophysical environments. The present work demonstrates that it can serve as a sensitive probe of nuclear structure as well. The recent TPC upgrade to GADGET II integrates the gaseous detector system with the FRIB Decay Station Initiator [45], enabling even more detailed and sensitive measurements in the future with both the Proton Detector (GADGET) and TPC (GADGET II) configurations.

Research at NSCL was funded by the National Science Foundation under grant Nos. PHY-1913554, PHY-1102511, PHY-1565546, PHY-1811855, PHY-2310059, and PHY-2110365, as well as by the Department of Energy Office of Science under Award No. DE-SC0016052. We acknowledge support from the Natural Sciences and Engineering Research Council of Canada (NSERC), as well as the Spanish MINECO grant AYA2017-86274-P, the E. U. FEDER funds, the AGAUR/Generalitat

de Catalunya grant No. SGR-661/2017, and the EU Horizon 2020 grant No. 101008324 ChETEC-INFRA. This article also benefited from discussions within the ChETEC COST Action (CA16117). Additional funding sources include Korean NRF grant No. RS-2024-00338255. We thank the NSCL staff for providing technical and administrative support for this experiment.

* budnerta@msu.edu

† wrede@frib.msu.edu

- [1] J. Hardy, L. Carraz, B. Jonson, and P. Hansen, The essential decay of pandemonium: A demonstration of errors in complex beta-decay schemes, *Physics Letters B* **71**, 307 (1977).
- [2] A. Kankainen, T. Eronen, S. P. Fox, H. O. U. Fynbo, U. Hager, J. Hakala, J. Huikari, D. G. Jenkins, A. Jokinen, S. Kopecky, I. Moore, A. Nieminen, H. Penttilä, S. Rinta-Antila, O. Tengblad, Y. Wang, and J. Äystö, Excited states in ^{31}S studied via beta decay of ^{31}Cl , *European Physical Journal A* **27**, 67 (2006).
- [3] A. Saastamoinen, *Studies of $T_z = -3/2$ Nuclei of Astrophysical Interest*, *Ph.D. thesis*, University of Jyväskylä (2011).
- [4] A. Saastamoinen, A. Kankainen, and L. Trache, Beta-decay of ^{31}Cl : an indirect probe of the $^{30}\text{P}(p, \gamma)^{31}\text{S}$ reaction. Present status and future perspectives, *European Physical Journal Plus* **131**, 272 (2016).
- [5] M. B. Bennett, C. Wrede, B. A. Brown, S. N. Liddick, D. Pérez-Loureiro, D. W. Bardayan, A. A. Chen, K. A. Chipps, C. Fry, B. E. Glassman, C. Langer, N. R. Larson, E. I. McNeice, Z. Meisel, W. Ong, P. D. O’Malley, S. D. Pain, C. J. Prokop, H. Schatz, S. B. Schwartz, S. Suchyta, P. Thompson, M. Walters, and X. Xu, Isospin Mixing Reveals $^{30}\text{P}(p, \gamma)^{31}\text{S}$ Resonance Influencing Nova Nucleosynthesis, *Phys. Rev. Lett.* **116**, 102502 (2016).
- [6] M. B. Bennett, C. Wrede, S. N. Liddick, D. Pérez-Loureiro, D. W. Bardayan, B. A. Brown, A. A. Chen, K. A. Chipps, C. Fry, B. E. Glassman, C. Langer, N. R. Larson, E. I. McNeice, Z. Meisel, W. Ong, P. D. O’Malley, S. D. Pain, C. J. Prokop, H. Schatz, S. B. Schwartz, S. Suchyta, P. Thompson, M. Walters, and X. Xu, Detailed study of the decay $^{31}\text{Cl}(\beta \gamma)^{31}\text{S}$, *Phys. Rev. C* **97**, 065803 (2018).
- [7] T. Budner, M. Friedman, C. Wrede, B. A. Brown, J. José, D. Pérez-Loureiro, L. J. Sun, J. Surbrook, Y. Ayyad, D. W. Bardayan, K. Chae, A. A. Chen, K. A. Chipps, M. Cortesi, B. Glassman, M. R. Hall, M. Janasik, J. Liang, P. O’Malley, E. Pollacco, A. Psaltis, J. Stomps, and T. Wheeler, Constraining the $^{30}\text{P}(p, \gamma)^{31}\text{S}$ Reaction Rate in O Ne Novae via the Weak, Low-Energy, β -Delayed Proton Decay of ^{31}Cl , *Physical Review Letters* **128**, 182701 (2022).
- [8] M. S. Basunia and A. Chakraborty, Nuclear Data Sheets for A=30, *Nuclear Data Sheets* **197**, 1 (2024).
- [9] J. Verotte, G. Berrier-Ronsin, S. Fortier, E. Hourani, A. Khendriche, J. M. Maison, L. H. Rosier, G. Rotbard, E. Caurier, and F. Nowacki, One-nucleon pickup reactions on ^{32}S : Experimental results and shell-model calculations, *Nuclear Physics A* **655**, 415 (1999).

- [10] Z. Ma, D. W. Bardayan, J. C. Blackmon, R. P. Fitzgerald, M. W. Guidry, W. R. Hix, K. L. Jones, R. L. Kozub, R. J. Livesay, M. S. Smith, J. S. Thomas, and D. W. Visser, Astrophysically important ^{31}S states studied with the $^{32}\text{S}(p, d)^{31}\text{S}$ reaction, *Phys. Rev. C* **76**, 015803 (2007).
- [11] C. Wrede, J. A. Caggiano, J. A. Clark, C. M. Deibel, A. Parikh, and P. D. Parker, Measurements of ^{31}S energy levels and reevaluation of the thermonuclear resonant $^{30}\text{P}(p, \gamma)^{31}\text{S}$ reaction rate, *Phys. Rev. C* **79**, 045803 (2009).
- [12] D. Irvine, A. A. Chen, A. Parikh, K. Setoodehnia, T. Faestermann, R. Hertenberg, H.-F. Wirth, V. Bildstein, S. Bishop, J. A. Clark, C. M. Deibel, J. Hendriks, C. Herlitzius, R. Krücken, W. N. Lennard, O. Lepyoshkina, R. Longland, G. Rugel, D. Seiler, K. Straub, and C. Wrede, Evidence for the existence of the astrophysically important 6.40-MeV state of ^{31}S , *Phys. Rev. C* **88**, 055803 (2013).
- [13] A. Kankainen, P. Woods, H. Schatz, T. Poxon-Pearson, D. Doherty, V. Bader, T. Baugher, D. Bazin, B. Brown, J. Browne, A. Estrade, A. Gade, J. José, A. Kontos, C. Langer, G. Lotay, Z. Meisel, F. Montes, S. Noji, F. Nunes, G. Perdikakis, J. Pereira, F. Recchia, T. Redpath, R. Stroberg, M. Scott, D. Seweryniak, J. Stevens, D. Weisshaar, K. Wimmer, and R. Zegers, Measurement of key resonance states for the $^{30}\text{P}(p, \gamma)^{31}\text{S}$ reaction rate, and the production of intermediate-mass elements in nova explosions, *Physics Letters B* **769**, 549 (2017).
- [14] C. Wrede, J. A. Caggiano, J. A. Clark, C. Deibel, A. Parikh, and P. D. Parker, New $^{30}\text{P}(p, \gamma)^{31}\text{S}$ resonances and oxygen-neon nova nucleosynthesis, *Phys. Rev. C* **76**, 052802(R) (2007).
- [15] A. Parikh, K. Wimmer, T. Faestermann, R. Hertenberg, J. José, R. Longland, H.-F. Wirth, V. Bildstein, S. Bishop, A. A. Chen, J. A. Clark, C. M. Deibel, C. Herlitzius, R. Krücken, D. Seiler, K. Straub, and C. Wrede, Improving the $^{30}\text{P}(p, \gamma)^{31}\text{S}$ rate in oxygen-neon novae: Constraints on J^π values for proton-threshold states in ^{31}S , *Phys. Rev. C* **83**, 045806 (2011).
- [16] A. Parikh, C. Wrede, and C. Fry, Toward concordance of E_x and J^π values for proton unbound ^{31}S states, *European Physical Journal Plus* **131**, 345 (2016).
- [17] D. G. Jenkins, C. J. Lister, M. P. Carpenter, P. Chowdhury, N. J. Hammond, R. V. F. Janssens, T. L. Khoo, T. Lauritsen, D. Seweryniak, T. Davinson, P. J. Woods, A. Jokinen, and H. Penttila, Mirror energy differences in the $A = 31$ mirror nuclei, ^{31}S and ^{31}P , and their significance in electromagnetic spin-orbit splitting, *Phys. Rev. C* **72**, 031303(R) (2005).
- [18] D. G. Jenkins, A. Meadowcroft, C. J. Lister, M. P. Carpenter, P. Chowdhury, N. J. Hammond, R. V. F. Janssens, T. L. Khoo, T. Lauritsen, D. Seweryniak, T. Davinson, P. J. Woods, A. Jokinen, H. Penttila, G. Martínez-Pinedo, and J. José, Reevaluation of the $^{30}\text{P}(p, \gamma)^{31}\text{S}$ astrophysical reaction rate from a study of the $T = 1/2$ mirror nuclei, ^{31}S and ^{31}P , *Phys. Rev. C* **73**, 065802 (2006).
- [19] D. T. Doherty, G. Lotay, P. J. Woods, D. Seweryniak, M. P. Carpenter, C. J. Chiara, H. M. David, R. V. F. Janssens, L. Trache, and S. Zhu, Key Resonances in the $^{30}\text{P}(p, \gamma)^{31}\text{S}$ Gateway Reaction for the Production of Heavy Elements in ONe Novae, *Phys. Rev. Lett.* **108**, 262502 (2012).
- [20] D. T. Doherty, P. J. Woods, G. Lotay, D. Seweryniak, M. P. Carpenter, C. J. Chiara, H. M. David, R. V. F. Janssens, L. Trache, and S. Zhu, Level structure of ^{31}S : From low excitation energies to the region of interest for hydrogen burning in novae through the $^{30}\text{P}(p, \gamma)^{31}\text{S}$ reaction, *Phys. Rev. C* **89**, 045804 (2014).
- [21] K. Setoodehnia, A. A. Chen, J. Chen, J. A. Clark, C. M. Deibel, J. Hendriks, D. Kahl, W. N. Lennard, P. D. Parker, D. Seiler, and C. Wrede, Level structure of ^{31}S via $^{32}\text{S}(p, d)^{31}\text{S}$, *Phys. Rev. C* **102**, 045806 (2020).
- [22] S. Burcher, K. A. Chipps, R. O. Hughes, C. S. Reingold, A. Saaastamoinen, J. T. Harke, N. Cooper, S. Ahn, J. M. Allmond, H. Clark, J. A. Cizewski, M. R. Hall, J. Hooker, H. Jayatissa, K. L. Jones, S. Ota, S. D. Pain, K. Schmidt, A. Simon, and S. Upadhyayula, Developing the $^{32}\text{S}(p, d)^{31}\text{S}^*(p)(\gamma)$ reaction to probe the $^{30}\text{P}(p, \gamma)^{31}\text{S}$ reaction rate in classical novae, *Phys. Rev. C* **105**, 045805 (2022).
- [23] L. Sun, C. Fry, B. Davids, N. Esker, C. Wrede, M. Alcorta, S. Bhattacharjee, M. Bowry, B. Brown, T. Budner, R. Caballero-Folch, L. Evitts, M. Friedman, A. Garnsworthy, B. Glassman, G. Hackman, J. Henderson, O. Kirsebom, J. Lighthall, P. Machule, J. Measures, M. Moukaddam, J. Park, C. Pearson, D. Pérez-Loureiro, C. Ruiz, P. Ruotsalainen, J. Smallcombe, J. Smith, D. Southall, J. Surbrook, L. Weghorn, and M. Williams, First application of Markov chain Monte Carlo-based Bayesian data analysis to the Doppler-shift attenuation method, *Physics Letters B* **839**, 137801 (2023).
- [24] J. Äystö, J. Honkanen, K. Vierinen, A. Hautojärvi, K. Eskola, and S. Messelt, Observation of beta-delayed protons in the decay of ^{31}Cl , *Physics Letters B* **110**, 437 (1982).
- [25] J. Äystö, P. Taskinen, K. Eskola, K. Vierinen, and S. Messelt, Studies of Weak Beta-Delayed Protons Emitted in the Decay of Odd-Z, $T_z = -3/2$ Nuclei, *Physica Scripta* **T5**, 193 (1983).
- [26] J. Äystö, X. J. Xu, D. M. Moltz, J. E. Reiff, J. Cerny, and B. H. Wildenthal, Beta-delayed proton decays of ^{27}P and ^{31}Cl : Gamow-Teller decays with large Q values, *Phys. Rev. C* **32**, 1700 (1985).
- [27] T. J. Ognibene, J. Powell, D. M. Moltz, M. W. Rowe, and J. Cerny, Additional results from the β -delayed proton decays of ^{27}P and ^{31}Cl , *Phys. Rev. C* **54**, 1098 (1996).
- [28] W. Mueller, J. Church, T. Glasmacher, D. Gutknecht, G. Hackman, P. Hansen, Z. Hu, K. Miller, and P. Quirin, Thirty-two-fold segmented germanium detectors to identify γ -rays from intermediate-energy exotic beams, *Nuclear Instruments and Methods in Physics Research Section A: Accelerators, Spectrometers, Detectors and Associated Equipment* **466**, 492 (2001).
- [29] A. Stolz, T. Baumann, T. Ginter, D. Morrissey, M. Portillo, B. Sherrill, M. Steiner, and J. Stetson, Production of rare isotope beams with the NSCL fragment separator, *Nuclear Instruments and Methods in Physics Research Section B: Beam Interactions with Materials and Atoms* **241**, 858 (2005).
- [30] D. Bazin, V. Andreev, A. Becerril, M. Doléans, P. Mantica, J. Ottarson, H. Schatz, J. Stoker, and J. Vincent, Radio Frequency Fragment Separator at NSCL, *Nuclear Instruments and Methods in Physics Research Section A: Accelerators, Spectrometers, Detectors and Associated Equipment* **606**, 314 (2009).
- [31] O. Tarasov and D. Bazin, LISE++: Radioactive beam production with in-flight separators, *Nuclear Instruments*

- and Methods in Physics Research Section B: Beam Interactions with Materials and Atoms **266**, 4657 (2008), proceedings of the XVth International Conference on Electromagnetic Isotope Separators and Techniques Related to their Applications.
- [32] E. Pollacco, L. Trache, E. Simmons, A. Spiridon, M. McCleskey, B. Roeder, A. Saastamoinen, R. Tribble, G. Pascovici, M. Kebbiri, J. Mols, and M. Raillot, AstroBox: A novel detection system for very low-energy protons from β -delayed proton decay, *Nuclear Instruments and Methods in Physics Research Section A: Accelerators, Spectrometers, Detectors and Associated Equipment* **723**, 102 (2013).
- [33] M. Friedman, D. Pérez-Loureiro, T. Budner, E. Pollacco, C. Wrede, M. Cortesi, C. Fry, B. Glassman, M. Harris, J. Heideman, M. Janasik, B. Roeder, M. Roosa, A. Saastamoinen, J. Stomps, J. Surbrook, P. Tiwari, and J. Yurkon, GADGET: a Gaseous Detector with Germanium Tagging, *Nuclear Instruments and Methods in Physics Research Section A: Accelerators, Spectrometers, Detectors and Associated Equipment* **940**, 93 (2019).
- [34] Y. Giomataris, P. Rebougeard, J. Robert, and G. Charpak, MICROMEGAS: a high-granularity position-sensitive gaseous detector for high particle-flux environments, *Nuclear Instruments and Methods in Physics Research Section A: Accelerators, Spectrometers, Detectors and Associated Equipment* **376**, 29 (1996).
- [35] J. F. Ziegler, M. Ziegler, and J. Biersack, SRIM – The stopping and range of ions in matter (2010), *Nuclear Instruments and Methods in Physics Research Section B: Beam Interactions with Materials and Atoms* **268**, 1818 (2010), 19th International Conference on Ion Beam Analysis.
- [36] C. Prokop, S. Liddick, B. Abromeit, A. Chemey, N. Larson, S. Suchyta, and J. Tompkins, Digital data acquisition system implementation at the National Superconducting Cyclotron Laboratory, *Nuclear Instruments and Methods in Physics Research Section A: Accelerators, Spectrometers, Detectors and Associated Equipment* **741**, 163 (2014).
- [37] G. Gilmore, Appendix D: Gamma-Ray Energies in the Detector Background and the Environment, in *Practical Gamma-Ray Spectrometry* (John Wiley & Sons, Ltd., 2008) pp. 361–364.
- [38] J. Chen and B. Singh, Nuclear Structure and Decay Data for A=31 Isobars, *Nuclear Data Sheets* **184**, 29 (2022).
- [39] J. Batchelder, Recommended values for β^+ -delayed proton and α emission, *Atomic Data and Nuclear Data Tables* **132**, 101323 (2020).
- [40] I. Ray, M. R. Basu, R. Kshetri, M. Saha Sarkar, S. Sarkar, P. Banerjee, S. Chattopadhyay, C. C. Dey, A. Goswami, J. M. Chatterjee, A. Mukherjee, S. Bhattacharya, B. Dasmahapatra, P. Datta, H. C. Jain, R. K. Bhowmik, S. Muralithar, and R. P. Singh, Indication of the onset of collectivity in ^{30}P , *Physical Review C* **76**, 034315 (2007).
- [41] B. Ramstein, L. H. Rosier, and R. J. De Meijer, Investigation of states in ^{30}P via the $^{30}\text{Si}(^3\text{He}, t)^{30}\text{P}$ reaction at 30 MeV, *Nuclear Physics A* **363**, 110 (1981).
- [42] J. C. Vermeulen, C. R. Bingham, D. Dijkhuizen, R. J. De Meijer, and L. Put, Investigation of the decay properties of high-spin two-nucleon states via the $^{28}\text{Si}(\alpha, d\gamma)^{30}\text{P}$ reaction at $E_\alpha = 50$ MeV, *Nuclear Physics A* **329**, 93 (1979).
- [43] C. E. Moss, C. Dètraz, and C. S. Zaidins, Beta decay of ^{26}Si , ^{30}S and ^{34}Ar , *Nuclear Physics A* **174**, 408 (1971).
- [44] M. Wang, W. Huang, F. Kondev, G. Audi, and S. Naimi, The AME 2020 atomic mass evaluation (II). Tables, graphs and references*, *Chinese Physics C* **45**, 030003 (2021).
- [45] R. Mahajan, T. Wheeler, E. Pollacco, C. Wrede, A. Adams, H. Alvarez-Pol, A. Andalib, A. Anthony, Y. Ayyad, D. Bazin, T. Budner, M. Cortesi, J. Dopfer, M. Friedman, B. Jain, A. Jaros, D. Pérez-Loureiro, B. Mehl, R. De Oliveira, S. Ravishankar, L. J. Sun, and J. Surbrook, Time projection chamber for GADGET II, *Phys. Rev. C* **110**, 035807 (2024).
- [46] F. Sauli, *Gaseous Radiation Detectors: Fundamentals and Applications*, Cambridge Monographs on Particle Physics, Nuclear Physics and Cosmology (Cambridge University Press, 2014).
- [47] S. Biagi, Monte Carlo simulation of electron drift and diffusion in counting gases under the influence of electric and magnetic fields, *Nuclear Instruments and Methods in Physics Research Section A: Accelerators, Spectrometers, Detectors and Associated Equipment* **421**, 234 (1999).
- [48] S. Raman and N. B. Gove, Rules for Spin and Parity Assignments Based on Logft Values, *Phys. Rev. C* **7**, 1995 (1973).
- [49] S. Turkat, X. Mougeot, B. Singh, and K. Zuber, Systematics of logft values for β^- , and EC/ β^+ transitions, *Atomic Data and Nuclear Data Tables* **152**, 101584 (2023).
- [50] J. Chen, RadiationReport, <https://github.com/IAEA-NSDDNetwork/RadiationReport> (2025).
- [51] A. Kankainen, A. Honkanen, K. Peräjärvi, and A. Saastamoinen, Decays of $T_Z = -3/2$ nuclei ^{23}Al , ^{31}Cl , and ^{41}Ti , *Hyperfine Interactions* **223**, 121 (2014).
- [52] A. Magilligan and B. A. Brown, New isospin-breaking “USD” Hamiltonians for the sd shell, *Phys. Rev. C* **101**, 064312 (2020).
- [53] J. C. Hardy and I. S. Towner, Superaligned $0^+ \rightarrow 0^+$ nuclear β decays: 2020 critical survey, with implications for V_{ud} and CKM unitarity, *Phys. Rev. C* **102**, 045501 (2020).
- [54] S. Navas, C. Amsler, T. Gutsche, C. Hanhart, J. J. Hernández-Rey, C. Lourenço, A. Masoni, M. Mikhasenko, R. E. Mitchell, *et al.* (Particle Data Group Collaboration), Review of Particle Physics, *Phys. Rev. D* **110**, 030001 (2024).
- [55] J. Davidson, D. Hutcheon, D. Gill, T. Taylor, D. Shepard, and W. Olsen, Energy levels of ^{31}S , *Nuclear Physics A* **240**, 253 (1975).
- [56] W. A. Richter, S. Mkhize, and B. A. Brown, sd -shell observables for the USDA and USDB Hamiltonians, *Phys. Rev. C* **78**, 064302 (2008).
- [57] M. Friedman, T. Budner, D. Pérez-Loureiro, E. Pollacco, C. Wrede, J. José, B. A. Brown, M. Cortesi, C. Fry, B. Glassman, J. Heideman, M. Janasik, M. Roosa, J. Stomps, J. Surbrook, and P. Tiwari, Low-energy ^{23}Al β -delayed proton decay and ^{22}Na destruction in novae, *Phys. Rev. C* **101**, 052802 (2020).
- [58] L. J. Sun, M. Friedman, T. Budner, D. Pérez-Loureiro, E. Pollacco, C. Wrede, B. A. Brown, M. Cortesi, C. Fry, B. E. Glassman, J. Heideman, M. Janasik, A. Kruskie, A. Magilligan, M. Roosa, J. Stomps, J. Surbrook, and P. Tiwari, ^{25}Si β^+ -decay spectroscopy, *Phys. Rev. C* **103**,

014322 (2021).